Analytical dispersion relation for forward volume spin waves in ferrimagnets near the angular momentum compensation condition

Luis Sánchez-Tejerina,[1] David Osuna Ruiz,[2] Víctor Raposo,[3,4]
Eduardo Martínez,[3,4] Luis López Díaz,[3,4] and Óscar Alejos[1]

[1]*Departamento de Electricidad y Electrónica, Universidad de Valladolid, Valladolid, Spain.**

[2]*Departamento de Ingeniería Eléctrica, Electrónica y de Comunicación, Universidad Pública de Navarra, Pamplona, Spain*

[3]*Departamento de Física Aplicada, Universidad de Salamanca, Salamanca, Spain*

[4]*Unidad de Excelencia en Luz y Materia Estructuradas (LUMES), Universidad de Salamanca, Salamanca, Spain*

(Dated: August 18, 2025)

Abstract

Antiferromagnetic magnonics has become the focus of intense scientific research because of the advantages of these materials compared to ferromagnets. However, ferrimagnetic materials have received much less attention despite exhibiting similar dynamical features at the angular momentum compensation point. In this paper, we present analytical expressions describing the dispersion relation of forward volume spin waves in ferrimagnetic materials near the angular momentum compensation point. We benchmark the derived dispersion relations against full micromagnetic simulations showing an excellent agreement between both approaches. We predict two different branches for forward volume spin waves in ferrimagnetic materials merging into a single branch at the angular momentum compensation point. Our results can assist in the design of magnonic devices built on ferrimagnetic materials.

I. INTRODUCTION

Magnon propagation in both antiferromagnetic (AFM) and ferrimagnetic (FiM) materials is being the subject of numerous studies in recent times [1–11] because of their particular characteristics in terms of higher frequency dynamics, minimal sensitivity to external fields, and the existence of a wide range of available materials, mostly electrical insulators, as compared to metallic ferromagnetic (FM) materials. Another important aspect is that the spin transport in AFM and FiM insulators (a key concept in spintronics) is primarily due to magnons, given the absence of conduction electrons, yet another difference with respect to most FM materials, where, being mostly conductors, electrons are the main spin carriers. This fact establishes an immediate connection between magnonics and spintronics. Furthermore, the absence of electron transport minimizes the importance of thermal effects from local heating [11].

Significant effort has been made to analytically describe the magnetization dynamics in magnetic materials. Kalinikos and Slavin's work on FM materials [12] established a precedent for analyzing spin wave dispersion across a broad frequency spectrum. In recent years, there has been a notable increase in theoretical studies of spin dynamics in AFM materials, mostly insulators. Among them, we can mention the characterization of the

* Contact author: luis.sanchez-tejerina@uva.es

fundamental resonance modes $k = 0$ [3–5], magnon propagation in uniform films [6, 13], or through material interfaces [14], or the interaction of AFM domain walls (DW) and magnons [1, 7], always focused on their fundamental physics, since knowledge of AFM magnonics is still scarce [3, 8, 15]. These materials could serve as a platform for developing magnonic oscillators and amplifiers [16] that could boost the ultrafast data transfer systems, or to generate magnon Bose-Einstein condensates for quantum computing [17]. On the other hand, FiM materials can mimic the dynamic response of AFMs at the angular momentum compensation (AMC) point [18–20], as well as interact with magnetic textures [21, 22], with the advantage that they are easier to manipulate and detect by electrical and/or optical means [23–25]. Indeed, localized precession of spins in FiM materials reaching sub-THz regimes, have been analytically predicted [2], with applications in high-frequency spintronic devices [26]. Spintronics also enables an easier control of spin order [27] and improves detection of magnetization dynamics in FiM [28, 29]. In contrast to FM materials, the fast dynamics (THz) of FiM systems due to the lack of inertia, when angular momentum is reduced, may lead to potential applications in ultra-fast or more energetically efficient devices as compared to FM [29–31]. Besides, the problem of large energy consumption of current neuromorphic computing networks can also be efficiently tackled by combining magnonic waveguides [32] and resonators [33, 34]. Finally, it is worth mentioning that in recent years developing ultra-fast artificial neural network circuitry with magnonics [33] and other non-conventional computing approaches [35] has raised attention.

A recent work of our group showed by means of micromagnetic simulations the possibility of exciting high-frequency ($\sim$ THz) propagating spin waves in FiM strips [10]. Such micromagnetic modeling, based on the interaction between two antiparallel coupled magnetic sublattices, predicted the existence of forward volume spin waves (FVSWs) in perpendicularly magnetized nanostrips, so that the main component of the net magnetization results perpendicular to the direction of SW propagation. Thus, in the case of spin angular momentum compensation between the two sublattices a single dispersion curve was obtained but, outside the angular momentum compensation condition, the dispersion relation splits into two curves whose separation was strongly influenced by the strength of the coupling between sublattices.

In this work, we obtain analytical expressions to account for the dispersion curves in these complex systems, modeling a generic FiM insulator near the AMC condition. To test the

accuracy of our theoretical predictions, a set of micromagnetic simulations have also been carried out, showing an excellent match between theory and the numerical results, then unveiling the origin of the mentioned complex behavior of these coupled systems.

II. ANALYTICAL CALCULATIONS

In our model the FiM is described as formed by two strongly coupled sub-lattices through the exchange interaction, each sub-lattice represented by respective magnetizations that are aligned along the directions of the unit vectors $\vec{m}_i$ $(i = 1, 2)$ at each point. In general, the energy functional includes symmetric exchange, Zeeman, magnetostatic, and anisotropy interactions. Antisymmetric exchange in the form of the Dzyaloshinkii-Moriya interaction can also be considered, but our calculations show that it is irrelevant for the modes discussed in this work. Additionally, no external field will be applied and magnetostatic effects are neglected, because of the relatively low value of the net magnetization. Nonetheless, we have tested the validity of the latter assumption comparing a subset of simulations with the corresponding ones including the demagnetizing field (see supplementary material S1 [36]). Accordingly, exchange energy density are expressed as [37–39]

$$\varepsilon_{\text{exch}} = A_{ii}||\nabla\vec{m}_1||^2 + A_{ii}||\nabla\vec{m}_2||^2 + A_{ij}\langle\nabla\vec{m}_1, \nabla\vec{m}_2\rangle - B_{ij}\vec{m}_1\vec{m}_2, \tag{1}$$

where $||M||$ represents the Frobenius norm of matrix M and $\langle M_1, M_2\rangle$ is the Frobenius inner product of matrices M_1 and M_2 which reads as the trace of the product of $M_1^\dagger$ and M_2. A_{ii} are the non-local intra-lattice exchange coefficients, while A_{ij} is the non-local inter-lattice exchange coefficient. As can be noted, the intralattice exchange parameter is assumed to be equal for both sublattices. Finally, B_{12} determines the strength of the local inter-lattice exchange [37]. Regarding the uniaxial anisotropy interaction, the expression

$$\varepsilon_{\text{anis}} = -K_u\left(\vec{m}_1 \cdot \vec{u}\right)^2 - K_u\left(\vec{m}_2 \cdot \vec{u}\right)^2 \tag{2}$$

is to be considered, $\vec{u}$ being the unit vector in the direction of the system easy axis ($K_u > 0$), which has been chosen as z axis. Again, the anisotropy constant is assumed to be the same for both sublattices. This simplifies calculations but including two different anisotropy constant can be done pretty straightforwardly. The final result is to weight the anisotropy contribution of each sublattice by the relative angular momentum density of each sublattice.

For the sake of completeness, the energy density, ε, also includes the Dzyaloshinkii-Moriya interaction (DMI) [37, 40]

$$\begin{aligned}\varepsilon_{\text{dmi}} = D_1 \left((\vec{m}_1 \cdot \vec{u}_n) \nabla \cdot \vec{m}_1 - \vec{m}_1 \cdot \nabla (\vec{m}_1 \cdot \vec{u}_n) \right) + \\ + D_2 \left((\vec{m}_2 \cdot \vec{u}_n) \nabla \cdot \vec{m}_2 - \vec{m}_2 \cdot \nabla (\vec{m}_2 \cdot \vec{u}_n) \right),\end{aligned} \tag{3}$$

although we will later prove that this interaction does not affect the dispersion relations for FVSW under the assumptions stated above. Finally, as commented above, the AMC condition occurs near the magnetization compensation point, so dipolar interactions are negligible (see supplementary material S1 [36]). Accordingly, the total energy density ε is written as the sum of $\varepsilon_{\text{exch}}$, $\varepsilon_{\text{anis}}$, and ε_{dmi}.

Within this model, magnetization dynamics is determined by two strongly coupled Landau-Lifshitz-Gilbert (LLG) equations [5, 10, 38]

$$\dot{\vec{m}}_i = -\gamma_i \vec{m}_i \times \vec{B}_{\text{eff},i} + \alpha_i \vec{m}_i \times \dot{\vec{m}}_i + \vec{\tau}_{\text{SC},i} \quad (i = 1, 2), \tag{4}$$

where γ_i and α_i are the gyromagnetic factor, and the damping parameter for each sub-lattice, respectively. γ_i is proportional to the free-electron gyromagnetic factor γ_e in the form $\gamma_i = \frac{g_i}{2}\gamma_e$, with g_i being the corresponding Landé factor for each sublattice. $\vec{B}_{\text{eff},i}$ is the effective field, calculated as $\vec{B}_{\text{eff},i} = -\frac{1}{M_{\text{S},i}} \frac{\delta \varepsilon}{\delta \vec{m}_i}$, where $M_{\text{S},i}$ is the saturation magnetization of sublattice i, and $\vec{\tau}_{\text{SC},i}$, corresponds to the torque associated with the angular-momentum injection (AMI) due to spin currents (SC). For the sake of concretion, to perform the micromagnetic simulations we assumed that the SC is due to the spin Hall effect [37, 41]. In that case, $\vec{\tau}_{\text{SC},i} = \gamma_i \frac{\hbar \theta_{SH} J}{2etM_{\text{S},i}} \vec{m}_i \times (\vec{m}_i \times \vec{p})$ where $\hbar$ is the reduced Planck constant, θ_{SH} is the spin Hall angle, e is the elementary charge, t the magnetic layer thickness and $\vec{p}$ is the direction of spin accumulation. The right-hand side of (4) then includes two complementary terms, Gilbert damping and AMI. These terms are complementary in the sense that they describe the flux of angular momentum in and out the spin system. These subsystems are usually conduction electrons or the mechanical degrees of freedom of the crystal lattice (such as lattice vibrations). Since the aim of this work is to compute the excitation modes of the magnetic system, detailing either how the system is excited or how it is damped is not relevant, so these terms can be ignored or assumed to compensate for each other. Harmonic excitation of angular frequency ω will also be assumed for the analytical derivation to obtain periodic solutions in the direction of propagation of the SWs with wavenumber k. Finally,

since the study focuses on narrow (one-dimensional) strips, the propagation direction will be taken along the direction of the strip, which can be assigned to the x-axis.

Under these assumptions, and for low excitation amplitudes, the respective magnetizations for each sublattice are expected to vary in time and space in the form $\vec{m}_i = \vec{m}_{i,eq} + \delta\vec{m}_i \mathrm{e}^{i(\omega t - kx)}$, where $\vec{m}_{i,eq}$ represents the equilibrium state for the magnetization, perpendicular to the strip, and $\delta\vec{m}_i$ is a small in-plane vector that describes the perturbation from equilibrium. This expression is to be applied to the resultant effective field $\vec{B}_{\mathrm{eff},i} = -\frac{1}{M_{\mathrm{S},i}}\frac{\delta\varepsilon}{\delta\vec{m}_i}$. Likewise, the effective field can be written as a sum of an equilibrium value plus a small harmonic value, that is,

$$\vec{B}_{eff,i} = \vec{B}_{i,eq} + \vec{B}_{i,dyn}\left(t,x\right). \tag{5}$$

Therefore, Eq. 4 can be written:

$$\begin{aligned} i\omega\delta\vec{m}_i = &-\gamma_i\left(\vec{m}_{i,eq}\times\vec{B}_{i,dyn}\right)e^{-i(\omega t-kx)} - \\ &-\gamma_i\left(\delta\vec{m}_i\times\vec{B}_{i,eq} + \delta\vec{m}_i\times\vec{B}_{i,dyn}\right), \end{aligned} \tag{6}$$

where the damping and antidamping term have been omitted. It should be noted that the addend $\vec{m}_{i,eq}\times\vec{B}_{i,eq} = 0$ as it is the torque at equilibrium. We can further simplify the expression by considering that the effective field at equilibrium is directed along $\pm\vec{u}_z$ and for small enough excitations we can assume $\delta\vec{m}_i \perp \vec{u}_z$. Consequently, Eq. 4 reduces to

$$\begin{aligned} i\omega\delta\vec{m}_i = &\pm\gamma_i\left(\left(\frac{B_{ij}}{M_{\mathrm{S},i}} - \frac{A_{ij}}{M_{\mathrm{S},i}}k^2\right)\delta\vec{m}_j - \frac{2A_{ii}}{M_{\mathrm{S},i}}k^2\delta\vec{m}_i\right)\times\vec{u}_z \pm \\ &\pm\gamma_i\left(\left(\frac{B_{ij}}{M_{\mathrm{S},i}} - \frac{2K_u}{M_{\mathrm{S},i}}\right)\delta\vec{m}_i\right)\times\vec{u}_z, \end{aligned} \tag{7}$$

after the second order terms in $\delta\vec{m}_i$ have been neglected. It is worth noting that, under these assumptions, the terms depending on the DMI no longer play any role in the dynamics as it was anticipated, because either they are second-order terms or dependent on the scalar product of $\delta\vec{m}_i$ and $\vec{u}_z$, vectors which have been assumed to be perpendicular. Consequently, any role played by DMI for FVSW in this configuration is a non-linear effect.

Considering the angular momentum densities $S_i = \frac{M_{\mathrm{S},i}}{\gamma_i}$, and after some algebra, we get

$$i\omega S_i\delta\vec{m}_i = \mp\left[\left(2K_u - B_{ij} + 2A_{ii}k^2\right)\delta\vec{m}_i - \left(B_{ij} - A_{ij}k^2\right)\delta\vec{m}_j\right]\times\vec{u}_z. \tag{8}$$

We can now recast this last result in terms of small magnetization $\vec{m}_+ = \vec{m}_1 + \vec{m}_2$ and Néel vector $\vec{l} = \vec{m}_1 - \vec{m}_2$, whose combined dynamic components can account for the dynamic

components of $\delta\vec{m}_1$ and $\delta\vec{m}_2$ in the form $\delta\vec{m}_1 = \dfrac{\delta\vec{m}_+ + \delta\vec{l}}{2}$ and $\delta\vec{m}_2 = \dfrac{\delta\vec{m}_+ - \delta\vec{l}}{2}$. Introducing $\nu_+ = \frac{S_1+S_2}{S_1S_2}$ and $\nu_- = \frac{S_1-S_2}{S_1S_2}$ as angular momentum decompensation factors, Eq. 8 transforms into the following couple of equations:

$$\begin{aligned} i\omega\delta\vec{m}_+ = \Bigg\{ & \nu_- \left[K_u - B_{ij} + \left(A_{ii} + \frac{A_{ij}}{2} \right) k^2 \right] \delta\vec{m}_+ - \\ & - \nu_+ \left[K_u + \left(A_{ii} - \frac{A_{ij}}{2} \right) k^2 \right] \delta\vec{l} \Bigg\} \times \vec{u}_z, \end{aligned} \tag{9a}$$

$$\begin{aligned} i\omega\delta\vec{l} = \Bigg\{ & -\nu_+ \left[K_u - B_{ij} + \left(A_{ii} + \frac{A_{ij}}{2} \right) k^2 \right] \delta\vec{m}_+ + \\ & + \nu_- \left[K_u + \left(A_{ii} - \frac{A_{ij}}{2} \right) k^2 \right] \delta\vec{l} \Bigg\} \times \vec{u}_z, \end{aligned} \tag{9b}$$

which is a set of coupled equations for the components of $\delta\vec{m}_+$ and $\delta\vec{l}$. The decoupling of the equations leads to the biquadratic equation in ω

$$\omega^4 - \left(2\nu_+^2 B + \nu_-^2 (A + C) \right) \frac{\omega^2}{4} + \frac{1}{16} \left(\nu_+^4 B^2 + \nu_-^4 AC - \nu_+^2 \nu_-^2 \left(AC + B^2 \right) \right) = 0, \tag{10}$$

whose solutions give the FVSW dispersion relations, constituting the main result of the work, are

$$\omega_\pm = \frac{1}{2} \sqrt{ \Gamma_A \Gamma_B \left(\nu_+^2 - \nu_-^2 \right) + \frac{1}{2} \left(\Gamma_A + \Gamma_B \right)^2 \nu_-^2 \left[1 \pm \sqrt{ \left(\frac{\Gamma_A - \Gamma_B}{\Gamma_A + \Gamma_B} \right)^2 + \frac{4\nu_+^2 \Gamma_A \Gamma_B}{\nu_-^2 \left(\Gamma_A + \Gamma_B \right)^2} } \right] }, \tag{11}$$

being Γ_A, and Γ_B,

$$\Gamma_A (k) = 2K_u + (2A_{ii} - A_{ij}) k^2, \tag{12a}$$

$$\Gamma_B (k) = 2 (K_u - B_{ij}) + (2A_{ii} + A_{ij}) k^2. \tag{12b}$$

Please notice that, in the case of two different anisotropy constant for each sublattice $K_{u,1} \neq K_{u,2}$ it would be necessary to substitute $K_u\nu_+$ by $\frac{S_1K_{u,2}+S_2K_{u,1}}{S_1S_2}$ and $K_u\nu_-$ by $\frac{S_1K_{u,2}-S_2K_{u,1}}{S_1S_2}$. Therefore, two frequencies $f_\pm = \omega_\pm / (2\pi)$ are possible for each k. Here, $\nu_\pm = \frac{1}{S_2} \pm \frac{1}{S_1}$ and $S_i = \frac{M_{S,i}}{\gamma_i}$ is the angular momentum density of the sublattices. As a result, the values of $f_\pm$ converge under AMC recovering the expression for the uniaxial AFM materials [42], $\omega = \frac{\sqrt{\Gamma_A\Gamma_B}}{S}$. This condition can be achieved either at a certain temperature for a given composition or for a certain composition at a given temperature. Additionally, the uniaxial FM dispersion relation is recovered [12] from Eq. 11 by considering equal angular momenta for both sub-lattices and setting to zero the inter-lattice exchange parameters, A_{ij} and B_{ij}.

III. MICROMAGNETIC SIMULATIONS SETUP

To prove the veracity of this result, we performed a series of numerical simulations based on a continuous approach, where the elementary volume contains two magnetization vectors, one for each sub-lattice, and both sub-lattices are coupled by an interlattice exchange interaction (see details in Ref. [43]). This continuous two sublattices approach has been used previously to describe the behavior of AFM and FiM materials [38, 39, 44, 45]. Such micromagnetic simulations take into account the same interactions as those considered for the analytical calculations, i.e., exchange (1), anisotropy (2), and DMI (3). Additionally, micromagnetic simulations can also account for dipolar interactions at the expense of a larger simulation cost. To check that the latter interaction is negligible, some simulations considering a dipolar field have been carried out (see supplementary material S1 [36]). Simulations of the modeled device (sketched in Fig. 1(a)) have been carried out using our code [38, 40, 43] implemented on graphic processing units. We note that Eq. 11 shows that the dispersion relation is determined by the angular momentum density of both sublattices, the anisotropy, and intra- and interlattice exchange parameters. Additionally, saturation magnetization for each sub-lattice can be adjusted varying the temperature and/or composition. Thus, this latter parameter is employed to define different angular momenta ratios [(i)-(iv)], summarized in Table I, near the AMC condition:

	$M_{S,1}$ [MA m^{-1}]	$M_{S,2}$ [MA m^{-1}]	S_1 [μJ s m^{-3}]	S_2 [μJ s m^{-3}]
(i)	1.094	1.044	39.08	36.35
(ii)	0.953	0.953	34.04	33.21
(iii)	0.887	0.909	31.67	31.67
(iv)	0.742	0.808	26.51	28.17

TABLE I. The four scenarios explored in simulations defined by different angular momenta and magnetization ratios.

Note that the magnetization compensation condition (ii) differs from the angular momentum compensation condition (iii) due to distinct Landé factors in each sublattice, $g_1 = 2$, $g_2 = 2.05$. Other parameters have been chosen to be the same for both sublattices, as the non-local intralattice exchange parameter, which is varied between 2 pJ m^{-1} and 40 pJ m^{-1}, and the local interlattice exchange parameter, which ranges from -1 MJ m^{-3} to -40 MJ m^{-3}.

It should be pointed out that the local (B_{ij}) and non-local (A_{ij}) interlattice exchange constants are not independent as both relate with the same exchange integral. However, this relation depends on the lattice constant and the number of sub-lattice neighbors, which differs for different crystals. For each value of B_{ij} we perform three simulations with different values of non-local exchange parameters, A_{ii} and A_{ij}. For large values of B_{ij}, it is possible to stabilize a uniform strip with virtually zero intralattice exchange ($A_{ii} = 0.1$ fJ m^{-1}). For those special cases, simulations with the latter intralattice exchange parameter have also been performed. The rest of significant parameters are those that can be found in the literature for a prototypical FiM as GdFeCo [18]: anisotropy constant $K_{u,i} = 0.1$MJ m^{-3} (refs. [46–49]), spin-Hall angle $\theta_{SH} = 0.15$ [38], and damping constant $\alpha_i = 0.001$. Also, a DMI parameter equal to $D = 0.12$ mJ m^{-3} has been considered. In any case, this parameter has no effect on the studied modes, as predicted by the analytical model. To further verify this statement, simulations with $D = 0.0$ mJ m^{-3} and $D = 1.20$ mJ m^{-3} are also provided in supplementary material S2 [50]. Please note that for large DMI parameters compared to the inhomogeneous exchange the ground state is no longer uniform, but a cycloid state is promoted [51]. In those cases, the assumptions of the model are no longer fulfilled, and the results cease to be valid.

The device under study consists of a FiM strip and a current line of a heavy metal (HM) that runs perpendicular to the strip at one end, as shown in Fig. 1(a). The FiM material is initially uniformly magnetized in the out-of-plane direction, z. The FiM strip area is 8192 nm $\times$ 32 nm, and is 6 nm thick, discretized in 1 nm $\times$ 1 nm $\times$ 6 nm cells, while the HM strip is 32 nm wide. Consequently, the 32 nm $\times$ 32 nm leftmost end surface of the FiM strip constitutes the excitation region of the device due to the SC generated via SOT from the HM. This SC is polarized along the $\pm\vec{u}_x$ direction depending on the instantaneous direction of the electric current along the HM strip. To excite the AFM strip, a sinc-shaped electric current pulse has been used, $J(t) = J_0 \mathrm{sinc}\left[2\pi f_c (t - t_c)\right]$, where $J_0 = 1$ TA m^{-2} is the pulse amplitude, t_c is a delay time, which has been chosen as one half of the total simulation time, set to 1 ns and f_c is the excitation cut-off frequency, which was set to 1 THz. This excitation configuration ensures that all frequencies below f_c are probed with a resolution of 1 GHz. Using this activation, we ensure that each mode is equivalently fed. In addition, this current is sufficiently small to remain in the linear regime of activation of damped, stable oscillations [4]. The delay time also provides a reasonable offset to the peak of the pulse,

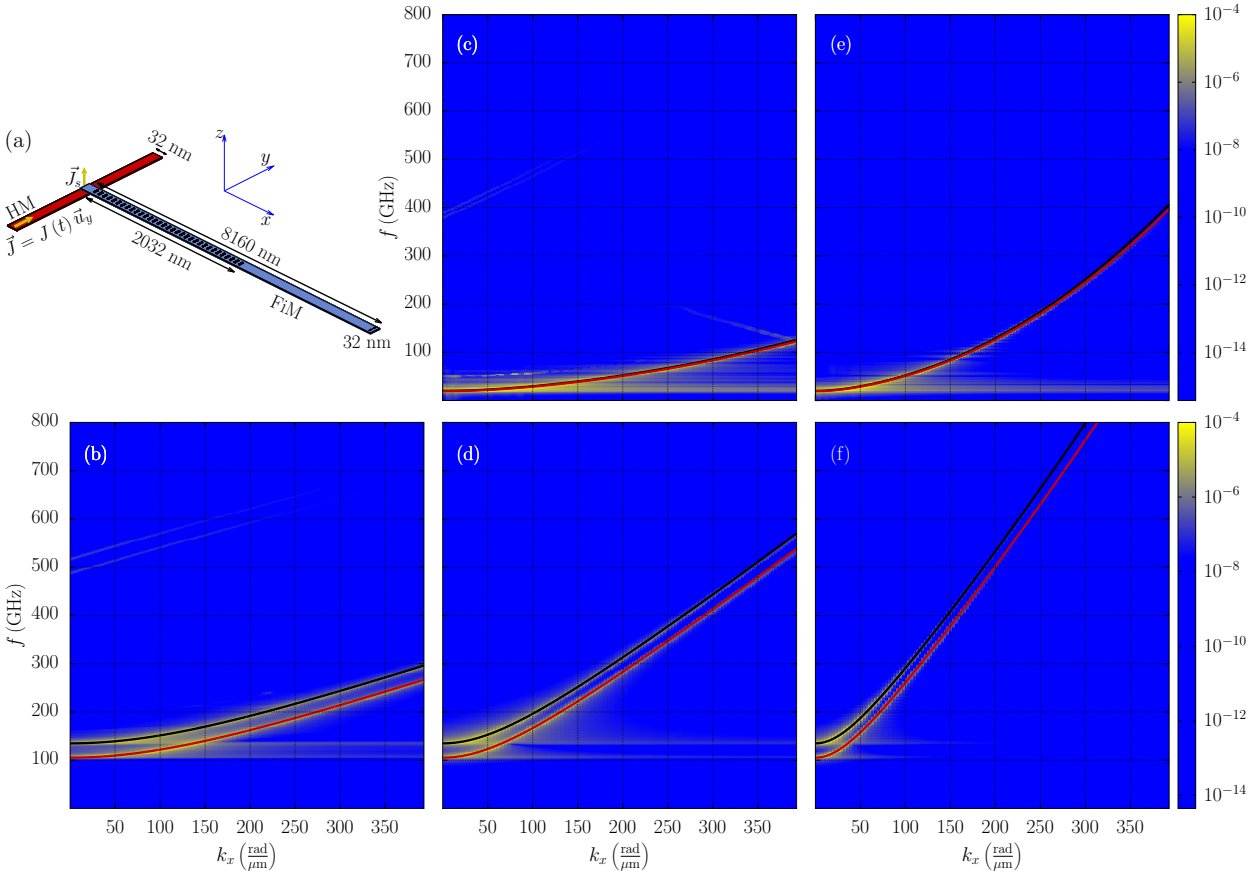

FIG. 1. (a) Sketch of the modeled device. (b)-(f) Dispersion diagrams of a FiM material obtained from n_x with sublattices angular momenta $S_1 = 1.025\, S_2 = 34.04$ µJ s m^{-3} for various intra- and intersublattices exchanges: (b) $A_{ii} = 0.1$ fJ m^{-1}, $A_{ij} = -6.0$ pJ m^{-1}, and $B_{ij} = -40$ MJ m^{-3} (c) $A_{ii} = 10$ pJ m^{-1}, $A_{ij} = -150$ fJ m^{-1}, and $B_{ij} = -1.0$ MJ m^{-3}, (d) $A_{ii} = 10$ pJ m^{-1}, $A_{ij} = -6.0$ pJ m^{-1}, and $B_{ij} = -40$ MJ m^{-3}, (e) $A_{ii} = 40$ pJ m^{-1}, $A_{ij} = -150$ fJ m^{-1}, and $B_{ij} = -1$ MJ m^{-3} , (f) $A_{ii} = 40$ pJ m^{-1}, $A_{ij} = -6.0$ pJ m^{-1}, and $B_{ij} = -40$ MJ m^{-3}. Colormaps are obtained from full micromagnetic simulations while solid lines corresponds to Eq. 11.

allowing a gradual increase in amplitude from the beginning of the simulation. To monitor the value of the local Néel vector $\vec{n} = \vec{m}_1 - \vec{m}_2$, a set of 254 regularly spaced probes is located on the FiM strip. The probes are 3 nm × 8 nm in size and 5 nm apart from each other, then occupying a total length of 2032 nm.

IV. VERIFICATION

A. Role of exchange parameter

To check the analytical expression given by Eq. 11 we first fixed the angular momenta ratio to Scenario (ii) $M_{\mathrm{S},1} = M_{\mathrm{S},2} = 0.953\ \mathrm{MA\,m^{-1}}$ and $S_1 = 1.025\ S_2 = 34.04\ \mu\mathrm{J\,s\,m^{-3}}$ corresponding to the magnetization compensation point. This allows us to clearly distinguish the two dispersion curves predicted from our calculations. We then study the effect of the different intra- and inter-lattice exchange parameters. As explained in subsection III, the non-local intralattice exchange parameter is varied between $2\ \mathrm{pJ\,m^{-1}}$ and $40\ \mathrm{pJ\,m^{-1}}$, and the local interlattice exchange parameter ranges from $-1\ \mathrm{MJ\,m^{-3}}$ to $-40\ \mathrm{MJ\,m^{-3}}$. Figure 1(b)-(f) depict the cases with lowest and largest intra- and interlattice exchange parameters in the considered range, as well as a case with a middle value of the intralattice exchange parameter. All combinations of parameters show an excellent agreement between Eq. 11 and full micromagnetic simulations in the whole range of frequencies and wave numbers. As predicted from the analytical expression, the effect of local interlattice exchange is double. First, a larger local interlattice exchange increases the frequency of the uniform precession, representing the minimum available frequency. This is translated into a shift of the whole branch towards higher frequencies, as can be checked by comparing Fig. 1(c) and (e) with Fig. 1(b),(d) and (f), thus increasing the phase velocity. In addition, the frequency difference between the two branches also increases for larger local interlattice exchanges. Moreover, as should be expected, non-local exchange, neither intralattice nor interlattice, affects the uniform mode as can be checked comparing Fig. 1(b) with Fig. 1(d) or (f) and Fig. 1(c) with Fig. 1(e). Nevertheless, those terms greatly affect the group velocity, being larger for larger non-local exchange parameter.

B. Role of uncompensated angular momenta density

To further corroborate the validity of Eq. 11 we now fix the intra- and interlattice exchange parameters to $A_{ii} = 10\ \mathrm{pJ\,m^{-1}}$, $A_{ij} = -1.5\ \mathrm{pJ\,m^{-1}}$, and $B_{ij} = -10\ \mathrm{MJ\,m^{-3}}$, and vary the angular momenta ratio. Figure 2 represents the dispersion relations for the four different specified scenarios, (i) $S_1 = 1.075\ S_2 = 39.08\ \mu\mathrm{J\,s\,m^{-3}}$, (ii) $S_1 = 1.025\ S_2 = 34.04\ \mu\mathrm{J\,s\,m^{-3}}$, (iii) $S_1 = S_2 = 31.67\ \mu\mathrm{J\,s\,m^{-3}}$, and (iv) $S_1 = 0.941\ S_2 = 26.51\ \mu\mathrm{J\,s\,m^{-3}}$. As expected,

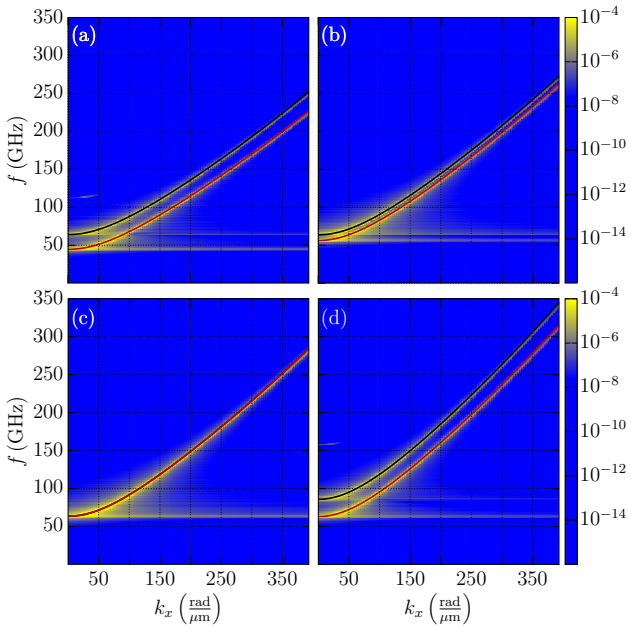

FIG. 2. Dispersion diagrams of a FiM material with exchange parameters: $A_{ii} = 10$ pJ m^{-1}, $A_{ij} = -1.5$ pJ m^{-1}, and $B_{ij} = -10$ MJ m^{-3} for different sublattices angular momenta relations: (a) $S_1 = 1.075\, S_2 = 39.08$ µJ s m^{-3} (i), (b) $S_1 = 1.025\, S_2 = 34.04$ µJ s m^{-3} (ii), (c) $S_1 = S_2 = 31.67$ µJ s m^{-3} (iii), (d) $S_1 = 0.941\, S_2 = 26.51$ µJ s m^{-3} (iv). Color maps are obtained from full micromagnetic simulations while solid lines correspond to Eq. 11.

at the AMC condition (iii), the two branches merge to a single one, and the larger the difference between the two sublattices angular momentum density, the larger the frequency shift between the two branches for a fixed wave number. In addition, the lower the angular momentum densities, the higher frequencies are reached. Nevertheless, we note that we have kept the energy densities constant. Finally, it should be noted that in all cases the agreement between Eq. 11 and the full micromagnetic simulations is excellent.

V. CONCLUSIONS

In conclusion, we have tested the analytical expression of the dispersion curves of FVSW in FiMs against numerical simulations of these materials, then revealing the dependencies of these curves on the different parameters governing magnetic dynamics in them. Since FiMs are considered as formed by two strongly coupled magnetic sublattices, there is a relevant role played by the inter-lattice exchange interactions, that impede from independently describing

the behavior of each sub-lattice. Two branches are found that converge as the system approaches the AMC condition. These analytical expressions quantify the role played by the uncompensation of the two sublattices near the AMC condition, giving a better insight on the underlying physical phenomena. In all cases, the work confirms the possibility of exciting high-frequency, close to the THz band, propagating AFM modes in FiM strips. Equation 11 also assists the choice of materials and composition/temperature to excite SWs with specific frequency and wavelength. Accordingly, the work facilitates the design of technological applications in this frequency range based on FiMs. Specifically, this makes it possible to implement logic devices based on SWs, as it will be the subject of a forthcoming work.

ACKNOWLEDGMENTS

We acknowledge funding from Project PID2023-150853NB-C31 funded by MICIU/AEI /10.13039/501100011033 and by European Union Next GenerationEU/PRTR.

[1] W. Wang, M. Albert, M. Beg, M.-A. Bisotti, D. Chernyshenko, D. Cortés-Ortuño, I. Hawke, and H. Fangohr, Magnon-Driven Domain-Wall Motion with the Dzyaloshinskii-Moriya Interaction. Physical Review Letters **114**, 087203 (2015).

[2] I. Lisenkov, R. Khymyn, J. Åkerman, N. X. Sun, and B. A. Ivanov, Subterahertz ferrimagnetic spin-transfer torque oscillator. Phys. Rev. B **100**, 100409 (2019).

[3] S. M. Rezende, A. Azevedo, and R. L. Rodríguez-Suárez, Introduction to antiferromagnetic magnons. Journal of Applied Physics **126**, 151101 (2019).

[4] R. Cheng, D. Xiao, and A. Brataas, Terahertz Antiferromagnetic Spin Hall Nano-Oscillator. Physical Review Letters **116**, 207603 (2016).

[5] V. Puliafito, R. Khymyn, M. Carpentieri, B. Azzerboni, V. Tiberkevich, A. Slavin, and G. Finocchio, Micromagnetic modeling of terahertz oscillations in an antiferromagnetic material driven by the spin Hall effect. Physical Review B **99**, 024405 (2019).

[6] X. Xu, Y. G. Semenov, and K. W. Kim, Electrical generation and propagation of spin waves in antiferromagnetic thin-film nanostrips. Applied Physics Letters **114**, 232403 (2019).

[7] R. Yanes, M. R. Rosa, and L. López-Díaz, Magnetic field control of antiferromagnetic domain walls in a thermal gradient. Physical Review B **102**, 134424 (2020).

[8] A. R. Safin, S. A. Nikitov, A. I. Kirilyuk, D. V. Kalyabin, A. V. Sadovnikov, P. A. Stremoukhov, M. V. Logunov, and P. A. Popov, Excitation of Terahertz Magnons in Antiferromagnetic Nanostructures: Theory and Experiment. Journal of Experimental and Theoretical Physics **131**, 71– (2020).

[9] C. Chen, C. Zheng, J. Zhang, and Y. Liu, Chirality reversal of resonant modes in GdFe ferrimagnets. Applied Physics Letters **123**, 212403 (2023).

[10] L. Sánchez-Tejerina, D. Osuna Ruiz, E. Martínez, L. López Díaz, V. Raposo, and Ó. Alejos, Spin waves in ferrimagnets near the angular magnetization compensation temperature: A micromagnetic study. Applied Physics Letters **125**, 082402 (2024).

[11] C. Kim, S. Lee, H.-G. Kim, J.-H. Park, K.-W. Moon, J. Y. Park, J. M. Yuk, K.-J. Lee, B.-G. Park, S. K. Kim, K.-J. Kim, and C. Hwang, Distinct handedness of spin wave across the compensation temperatures of ferrimagnets. Nature Materials **19**, 980 (2020).

[12] B. A. Kalinikos and A. N. Slavin, Theory of dipole-exchange spin wave spectrum for ferromagnetic films with mixed exchange boundary conditions. Journal of Physics C: Solid State Physics **19**, 7013 (1986).

[13] F. Millo, J.-P. Adam, C. Chappert, J.-V. Kim, A. Mouhoub, A. Solignac, and T. Devolder, Unidirectionality of spin waves in synthetic antiferromagnets. Physical Review Applied **20**, 054051 (2023).

[14] O. Y. Gorobets, V. V. Kulish, and I. A. Syzon, Theory of propagation of nonlinear spin wave through an antiferromagnetic magnonic crystal with four-sublattice interfaces Journal of Magnetism and Magnetic Materials. **587**, 171266 (2023).

[15] A. Barman, G. Gubbiotti, S. Ladak, A. O. Adeyeye, M. Krawczyk, J. Gräfe, C. Adelmann, S. Cotofana, A. Naeemi, V. I. Vasyuchka, B. Hillebrands, S. A. Nikitov, H. Yu, D. Grundler, A. V. Sadovnikov, A. A. Grachev, S. E. Sheshukova, J.-Y. Duquesne, M. Marangolo, G. Csaba, W. Porod, V. E. Demidov, S. Urazhdin, S. O. Demokritov, E. Albisetti, D. Petti, H. S. R. Bertacco, V. V. Kruglyak, V. D. Poimanov, S. Sahoo, J. Sinha, H. Yang, M. Münzenberg, T. Moriyama, S. Mizukami, P. Landeros, R. A. Gallardo, G. Carlotti, J.-V. Kim, R. L. Stamps, R. E. Camley, B. Rana, Y. Otani, W. Yu, T. Yu, G. E. W. Bauer, C. Back, G. S. Uhrig, O. V. Dobrovolskiy, B. Budinska, H. Qin, S. van Dijken, A. V. Chumak, A. Khitun, D. E. Nikonov,

I. A. Young, B. W. Zingsem, and M. Winklhofer, The 2021 Magnonics Roadmap. Journal of Physics: Condensed Matter **33**, 413001 (2021).

[16] Z. Zhang, Y.-C. Chien, M. T. Wong, F. Y. Gao, Z.-J. Liu, X. Ma, S. Cao, E. Baldini, and K. A. Nelson, Terahertz stimulated parametric downconversion of a magnon mode in an antiferromagnet. Science Advances **11**, eadv3757 (2025).

[17] S. O. Demokritov, V. E. Demidov, O. Dzyapko, G. A. Melkov, A. A. Serga, B. Hillebrands, and A. N. Slavin, Terahertz stimulated parametric downconversion of a magnon mode in an antiferromagnet. Nature **443**, 430 (2006).

[18] L. Caretta, M. Mann, F. Büttner, K. Ueda, B. Pfau, C. M. Günther, P. Hessing, A. Churikova, C. Klose, M. Schneider, D. Engel, C. Marcus, D. Bono, K. Bagschik, S. Eisebitt, and G. S. D. Beach, Fast current-driven domain walls and small skyrmions in a compensated ferrimagnet. Nature Nanotechnology **3** (2018).

[19] S. A. Siddiqui, J. Han, J. T. Finley, C. A. Ross, and L. Liu, Current-induced domain wall motion in a compensated ferrimagnet. Physical Review Letters **121**, 057701 (2018).

[20] F. Cutugno, L. Sanchez-Tejerina, R. Tomasello, M. Carpentieri, and G. Finocchio, Micromagnetic understanding of switching and self-oscillations in ferrimagnetic materials. Applied Physics Letters **118**, 052403 (2021).

[21] A. Donges, N. Grimm, F. Jakobs, S. Selzer, U. Ritzmann, U. Atxitia, and U. Nowak, Unveiling domain wall dynamics of ferrimagnets in thermal magnon currents: Competition of angular momentum transfer and entropic torque. Phys. Rev. Res. **2**, 013293 (2020).

[22] Y. Liu, T. Liu, Q. Yang, G. Tian, Z. Hou, D. Chen, Z. Fan, M. Zeng, X. Lu, X. Gao, M. Qin, and J. Liu, Design of controllable magnon frequency comb in synthetic ferrimagnets. Phys. Rev. B **109**, 174412 (2024).

[23] K. Ueda, M. Mann, C.-F. Pai, A.-J. Tan, and G. S. D. Beach, Spin-orbit torques in Ta/Tb_xCo_{100-x} ferrimagnetic alloy films with bulk perpendicular magnetic anisotropy. Applied Physics Letters **109**, 232403 (2016).

[24] K. Fleischer, N. Thiyagarajah, Y.-C. Lau, D. Betto, K. Borisov, C. C. Smith, I. V. Shvets, J. M. D. Coey, and K. Rode, Magneto-optic Kerr effect in a spin-polarized zero-moment ferrimagnet. Phys. Rev. B **98**, 134445 (2018).

[25] J. R. Hortensius, D. Afanasiev, M. Matthiesen, R. Leenders, R. Citro, A. V. Kimel, R. V. Mikhaylovskiy, B. A. Ivanov, and A. D. Caviglia, Coherent spin-wave transport in an antifer-

romagnet. Nature Physics **17**, 1001 (2021).

[26] R. E. Troncoso, K. Rode, P. Stamenov, J. M. D. Coey, and A. Brataas, Antiferromagnetic single-layer spin-orbit torque oscillators. Phys. Rev. B **99**, 054433 (2019).

[27] J. Ni, Z. Zhang, J. Lu, Q. Du, Z. Jiang, and L. Bellaiche, Nonvolatile Magnonics in Bilayer Magnetic Insulators. Nano Letters **25**, 1207 (2025).

[28] A. V. Chumak, P. Kabos, M. Wu, C. Abert, C. Adelmann, A. O. Adeyeye, J. Åkerman, F. G. Aliev, A. Anane, A. Awad, C. H. Back, A. Barman, G. E. W. Bauer, M. Becherer, E. N. Beginin, V. A. S. V. Bittencourt, Y. M. Blanter, P. Bortolotti, I. Boventer, D. A. Bozhko, S. A. Bunyaev, J. J. Carmiggelt, R. R. Cheenikundil, F. Ciubotaru, S. Cotofana, G. Csaba, O. V. Dobrovolskiy, C. Dubs, M. Elyasi, K. G. Fripp, H. Fulara, I. A. Golovchanskiy, C. Gonzalez-Ballestero, P. Graczyk, D. Grundler, P. Gruszecki, G. Gubbiotti, K. Guslienko, A. Haldar, S. Hamdioui, R. Hertel, B. Hillebrands, T. Hioki, A. Houshang, C.-M. Hu, H. Huebl, M. Huth, E. Iacocca, M. B. Jungfleisch, G. N. Kakazei, A. Khitun, R. Khymyn, T. Kikkawa, M. Kläui, O. Klein, J. W. Kłos, S. Knauer, S. Koraltan, M. Kostylev, M. Krawczyk, I. N. Krivorotov, V. V. Kruglyak, D. Lachance-Quirion, S. Ladak, R. Lebrun, Y. Li, M. Lindner, R. Macêdo, S. Mayr, G. A. Melkov, S. Mieszczak, Y. Nakamura, H. T. Nembach, A. A. Nikitin, S. A. Nikitov, V. Novosad, J. A. Otálora, Y. Otani, A. Papp, B. Pigeau, P. Pirro, W. Porod, F. Porrati, H. Qin, B. Rana, T. Reimann, F. Riente, O. Romero-Isart, A. Ross, A. V. Sadovnikov, A. R. Safin, E. Saitoh, G. Schmidt, H. Schultheiss, K. Schultheiss, A. A. Serga, S. Sharma, J. M. Shaw, D. Suess, O. Surzhenko, K. Szulc, T. Taniguchi, M. Urbánek, K. Usami, A. B. Ustinov, T. van der Sar, S. van Dijken, V. I. Vasyuchka, R. Verba, S. V. Kusminskiy, Q. Wang, M. Weides, M. Weiler, S. Wintz, S. P. Wolski, and X. Zhang, Advances in Magnetics Roadmap on Spin-Wave Computing. IEEE Transactions on Magnetics **58**, 1 (2022).

[29] Y. Zhang, X. Feng, Z. Zheng, Z. Zhang, K. Lin, X. Sun, G. Wang, J. Wang, J. Wei, P. Vallobra, Y. He, Z. Wang, L. Chen, K. Zhang, Y. Xu, and W. Zhao, Ferrimagnets for spintronic devices: From materials to applications. Applied Physics Reviews **10**, 011301 (2023).

[30] J. Liu, T. Xu, H. Feng, L. Zhao, J. Tang, L. Fang, and W. Jiang, Compensated Ferrimagnet Based Artificial Synapse and Neuron for Ultrafast Neuromorphic Computing. Advanced Functional Materials **32**, 2107870 (2022).

[31] C. Reinhoffer, I. Razdolski, C. Kadlec, P. Stein, F. Kadlec, S. Germanskiy, A. Stupakiewicz, P. H. M. van Loosdrecht, and E. A. Mashkovich, Terahertz excitation of exchange mode in a cavity formed by crystal interfaces. Phys. Rev. B **111**, 184412 (2025).

[32] V. Tikhonov, A. Ptashenko, and A. Sadovnikov, Anisotropy of waveguide modes of exchange spin waves in in-plane magnetized YIG films. Journal of Magnetism and Magnetic Materials **627**, 173117 (2025).

[33] K. G. Fripp, Y. Au, A. V. Shytov, and V. V. Kruglyak, Nonlinear chiral magnonic resonators: Toward magnonic neurons. Applied Physics Letters **122**, 172403 (2023).

[34] M. Xu, C. Hua, Y. Chen, and W. Yu, Frequency modulation on magnons in synthetic dimensions. Nature Communications **16** (2025).

[35] A. Papp, W. Porod, and G. Csaba, Nanoscale neural network using non-linear spin-wave interference. Nature Communications **12**, 6422 (2021).

[36] See Supplemental Material at [URL will be inserted by publisher] for a study of the effect of the demagnetizing field in the cases considered, showing a negligible contribution to the magnetization dynamics.

[37] L. Sánchez-Tejerina, V. Puliafito, P. Amiri, M. Carpentieri, and G. Finocchio, Dynamics of domain-wall motion driven by spin-orbit torque in antiferromagnets. Physical Review B **101**, 014433 (2020).

[38] E. Martínez, V. Raposo, and Ó. Alejos, Current driven domain wall dynamics in ferrimagnetic strips explained by means of a two interacting sublattices model. AIP Advances **10**, 015202 (2020).

[39] Z. Zheng, Y. Zhang, V. Lopez-Dominguez, L. Sánchez-Tejerina, J. Shi, X. Feng, L. Chen, Z. Wang, Z. Zhang, K. Zhang, B. Hong, Y. Xu, Y. Zhang, M. Carpentieri, A. Fert, G. Finocchio, W. Zhao, and P. Khalili Amiri, Field-free spin-orbit torque-induced switching of perpendicular magnetization in a ferrimagnetic layer with a vertical composition gradient. Nature Communications **12**, 4555 (2021).

[40] E. Martínez, V. Raposo, and Ó. Alejos, Current-driven domain wall dynamics in ferrimagnets: Micromagnetic approach and collective coordinates model. Journal of Magnetism and Magnetic Materials **491**, 165545 (2019).

[41] S. Emori, E. Martínez, k. J. Lee, H.-W. Lee, U. Bauer, S.-M. Ahn, P. A. adn D. C. Bono, and G. S. D. Beach, Spin Hall torque magnetometry of Dzyaloshinskii domain walls. Physical

Review B **90**, 184427 (2014).

[42] See for example eq. (36b) from [3], taking into account that the micromagnteic approach is only valid for low k and that expression is limitted to small anisotropy.

[43] E. Martínez, V. Raposo, and Ó. Alejos, Novel interpretation of recent experiments on the dynamics of domain walls along ferrimagnetic strips. Journal of Physics: Condensed Matter **32**, 465803 (2020).

[44] H.-A. Zhou, Y. Dong, T. Xu, K. Xu, L. Sánchez-Tejerina, L. Zhao, Y. Ba, P. Gargiani, M. Valvidares, Y. Zhao, M. Carpentieri, O. A. Tretiakov, X. Zhong, G. Finocchio, S. K. Kim, and W. Jiang, Compensated magnetic insulators for extremely fast spin-orbitronics. (2019), arXiv:1912.01775 [cond-mat.mtrl-sci].

[45] S. Arpaci, V. Lopez-Dominguez, J. Shi, L. Sánchez-Tejerina, F. Garesci, C. Wang, X. Yan, V. K. Sangwan, M. A. Grayson, M. C. Hersam, G. Finocchio, and P. Khalili Amiri, Observation of current-induced switching in non-collinear antiferromagnetic IrMn3 by differential voltage measurements. Nature Communications **12**, 3828 (2021).

[46] S. Joo, R. S. Alemayehu, J.-G. Choi, B.-G. Park, and G.-M. Choi, Magnetic anisotropy and damping constant of ferrimagnetic GdCo alloy near compensation point. Materials **14**, 2604 (2021).

[47] D.-H. Kim, T. Okuno, S. K. Kim, S.-H. Oh, T. Nishimura, Y. Hirata, Y. Futakawa, H. Yoshikawa, A. Tsukamoto, Y. Tserkovnyak, Y. Shiota, T. Moriyama, K.-J. Kim, K.-J. Lee, and T. Ono, Low magnetic damping of ferrimagnetic GdFeCo alloys. Physical Review Letters **122**, 127 (2019).

[48] G. Sala, C.-H. Lambert, S. Finizio, V. Raposo, V. Krizakova, G. Krishnaswamy, M. Weigand, J. Raabe, M. D. Rossell, E. Martinez, and P. Gambardella, Asynchronous current-induced switching of rare-earth and transition-metal sublattices in ferrimagnetic alloys. Nature Materials **21**, 640 (2022).

[49] T. Kato, K. Nakazawa, R. Komiya, N. Nishizawa, S. Tsunashima, and S. Iwata, Compositional dependence of g-factor and damping constant of GdFeCo amorphous alloy films. IEEE Transactions on Magnetics **44**, 3380 (2008).

[50] See Supplemental Material at [URL will be inserted by publisher] for a study of the effect of the DMI field in the cases considered, showing a negligible contribution to the magnetization dynamics.

[51] R. Tomasello, L. Sanchez-Tejerina, V. Lopez-Dominguez, F. Garescì, A. Giordano, M. Carpentieri, P. K. Amiri, and G. Finocchio, Domain periodicity in an easy-plane antiferromagnet with Dzyaloshinskii-Moriya interaction. Phys. Rev. B **102**, 224432 (2020).